Electronic Supplementary Information

Weak Acid-Responsive Porous Polyelectrolyte Membranes for Zinc Anode Interfaces

Wenbin Li[a], Changhao Wang[bc], Wenxuan Hu[a], Yongkang Wang[a], Congcong Li[a], Xiao Liu[a], Linyan Su[a], Beibei Yang[a]*, YunsongLi [b]*, Duan Bin[a]*and Hongbin Lu[a]*

[a] Department of Polymer Materials and Science, College of Chemistry and Chemical Engineering, Nantong University, Nantong, 226019, China

[b] Zhejiang Laboratory, Hangzhou 311100, P. R. China

[c] School of Materials Science and Engineering, Northwestern Polytechnical University, Xi'an 710072, P. R. China

* E-mail: yangbeibei@ntu.edu.cn, ysli@zhejianglab.com, dbin17@fudan.edu.cn, luhb@ntu.edu.cn (Hongbin Lu)

Experimental Procedures

Materials

Polyethyleneimine (PEI), sodium polystyrene sulfonate (PSSNa) and zinc sulfate heptahydrate ($ZnSO_4 \cdot 7H_2O$) were purchased from Shanghai Aladin Bio-Chem Technology Co., Ltd. Pyrene-4,5,9,10 tetrone (PTO) was purchased from Shanghai Tensus Biotech Co., Ltd.

Preparation of PEI-PSSNa coating and PSSNa coating

Firstly, 1.5 g of polyethyleneimine (PEI) was added into a mixture of 1.63 g of sodium polystyrene sulfonate (PSSNa) and 6.5 mL of deionized water. Subsequently, the mixture was evenly coated onto the zinc foil and copper foil that had been sanded with sandpaper. Then, the coatings underwent a drying process for a duration of 18 hours at ambient temperature. It is noteworthy that PSSNa coatings can be prepared in a similar manner, albeit without the incorporation of PEI in the mixture.

Fabrication of cathode materials

The cathode material was obtained by mixing and milling the active materials pyrene-4,5,9,10-tetrone (PTO), Kochin black (KB) and polytetrafluoroethylene (PTFE) binder in the ratio of 6:3:1 by weight for a period of one hour to make a homogeneous mixture.

Electrochemical measurement

The embedding/stripping properties of Zn ions in CR2016 button cell batteries were investigated in an open environment using glass fiber as membrane and 2 M ZnSO4 as electrolyte. The assembly of symmetrical cells was achieved by using bare Zn, Zn@PEI-PSSNa and Zn@PSSNa electrodes as working and counter electrodes, respectively. Conversely, for the assembly of asymmetric cells, bare Cu and Cu@PEIPSSNa electrodes were used as working electrodes and bare Zn as counter electrode. A complete battery can be assembled using PTO as the positive material and Zn@PEI-PSSNa or bare Zn as the negative electrode. The charge/discharge curves of the batteries were recorded at constant current using a Land CT3002A battery tester at room temperature. The operating voltage range of the full cell was 0.4 V to 1.6 V. Tafel curves, linear sweep voltammetry (LSV), electrochemical impedance spectroscopy (EIS), cyclic voltammetry (CV) and time variant analysis (CA) were performed using a Zn||Zn symmetric cell electrochemical workstation (CHI660E) system. In these tests, electrochemical impedance spectroscopy (EIS) was performed over a frequency range of 0.1-10^5 Hz, cyclic voltammetry (CV) was performed at a sweep rate of 1 mV/s over the range 0.4 V to 1.6 V, and a fixed overpotential of -150 mV was set for the measurement of time-varying current (CA) plots using a symmetric cell.

Materials Characterization

The chemical structure of the coating was analyzed using a Thermo Scientific Nicolet iS20 Fourier Transform Infrared Spectrometer (FT-IR). The microscopic morphology of the samples was determined by scanning electron microscopy (SEM) using a Gemini 300 and a JOEL JSM-6510. The crystal structure of the samples was determined using a Bruker D8 Advance X-ray diffractometer (XRD). A Nanofocus µsurf mobile high resolution confocal microscope (HRCM) was used to accurately characterize the 3D surface morphology of the samples. The morphological changes of symmetrical cells with bare Zn and Zn@PEI-PSSNa as electrodes were observed in situ during electroplating using a Zeiss Axio Imager M2m optical microscope.

Computational details

All DFT calculations were performed using the first-principles method software package VASP code based on density functional theory. The exchange correlation interactions between electrons were approximately described by generalized gradient approximation (GGA) with Perdew-Burke-Ernzerhof (PBE) functional, and the interaction between ions and electrons can be described by projector augmented plane-wave (PAW) pseudopotential. The exchange-correlation functional is modified by incorporating the optB88-vdW approach to account for long-range interactions between particles, specifically addressing the van der Waals corrections. The plane wave cutoff energy was set to be 600 eV. The convergence accuracy of energy and interatomic force during structural relaxation is set to 10^{-5} eV and 10^{-3}eV/Å respectively. The Brillouin zone was sampled using the Monkhorst-Pack scheme with a k-point 1×1×1 mesh. The transition state calculations were conducted using the climbing-image nudged elastic band (CI-NEB) method. In order to accurately describe the adsorption energy, we considered the influence of solvation effect and used VASPSol module to simulate the solvent environment, the dielectric constant (ε) was set to 78.35 to consider the solvation effect of water.

The binding energy (E_b) of Zn^{2+} and H_2O, PEI, PSSNa and PEI-PSSNa is defined as follows:

$$E_{\mathrm{b}} = E(\mathrm{A/Zn}^{2+}) - E(\mathrm{A}) - E(\mathrm{Zn}^{2+})$$

where $E(A/Zn^{2+})$ is the total energy of Zn^{2+} and H2O, PEI, PSSNa and PEI-PSSNa. $E(A)$ is the energy of H_2O, PEI, PSSNa and PEI-PSSNa.

The simulation of the electric field and concentration field was performed using the COMSOL Multiphysics software. Prior to the simulation, geometric models for the bare Zn electrode and the Zn electrode with a PSSNa or PEI-PSSNa layer were constructed. The protuberances on the surface of the pristine Zn electrode were modeled with a diameter of 0.8 μm and a height of 0.4 μm. Furthermore, the PSSNa or PEI-PSSNa interface layer was represented by a rectangular structure with porous channels, having a thickness of 1.5 μm. These channels were designed to simulate zinc ion transport pathways. The simulation was conducted based on the following partial differential equations:

$E = -\nabla V$

$J_i = -D_i \nabla c_i - z_i \mu_{m,\,i} F c_i E$

$\partial c_i / \partial t = -\nabla \cdot J_i$

where E is the electric field (V), V is the electric potential (V), J_i is the flux vector (mol m^{-2} s^{-1}), D_i is the diffusion coefficient (m^{2} s^{-1}), c_i is the concentration (mol m^{-3}), z_i is the charge number, $\mu_{m,\,i}$ is the ion mobility (mol s kg^{-1}) and F is the Faraday constant.

In this study, all-atom molecular dynamics (MD) simulations were performed using the LAMMPS software package to investigate the solvation behavior of Zn^{2+} ions in an aqueous solution containing PEI-PSSNa polymer chains. The simulation system was constructed in a cubic box with dimensions of 6×6×6 nm^3, containing 5570 water molecules, 200 pairs of $ZnSO_4$, and 10 PEI-PSSNa polymer chains. To simplify the system, Na^+ and Cl^- ions were excluded from the simulation. Periodic boundary conditions were applied in all three spatial directions. Interatomic interactions were described using the AMBER force field, and atomic partial charges were derived using the RESP (Restrained Electrostatic Potential) method to ensure accurate charge distribution.The simulation procedure consisted of three main stages: (i) energy minimization under the NVT ensemble, (ii) a 1 ns pre-equilibration at 300 K, and (iii) a 20 ns production run under the NPT ensemble at 300 K and 1 atm. Long-range electrostatic interactions were treated using the particle–particle particle–mesh (PPPM) method. After confirming that the system reached thermodynamic equilibrium, structural and dynamical analyses were carried out.

In this study, all-atom molecular dynamics (MD) simulations were performed using the LAMMPS software package to investigate the solvation behavior of Zn^{2+} ions in an aqueous solution containing PEI-PSSNa polymer chains. The simulation system was constructed in a cubic box with dimensions of $6 \times 6 \times 6$ nm^3, containing 5570 water molecules, 200 pairs of $ZnSO_4$, and 10 PEI-PSSNa polymer chains. To simplify the system, Na^+ and Cl^- ions were excluded from the simulation. Periodic boundary conditions were applied in all three spatial directions. Interatomic interactions were described using the AMBER force field, and atomic partial charges were derived using the RESP (Restrained Electrostatic Potential) method to ensure accurate charge distribution.The simulation procedure consisted of three main stages: (i) energy minimization under the NVT ensemble, (ii) a 1 ns pre-equilibration at 300 K, and (iii) a 20 ns production run under the NPT ensemble at 300 K and 1 atm. Long-range electrostatic interactions were treated using the particle–particle particle–mesh (PPPM) method. After confirming that the system reached thermodynamic equilibrium, structural and dynamical analyses were carried out.

Supplementary Figures and Tables

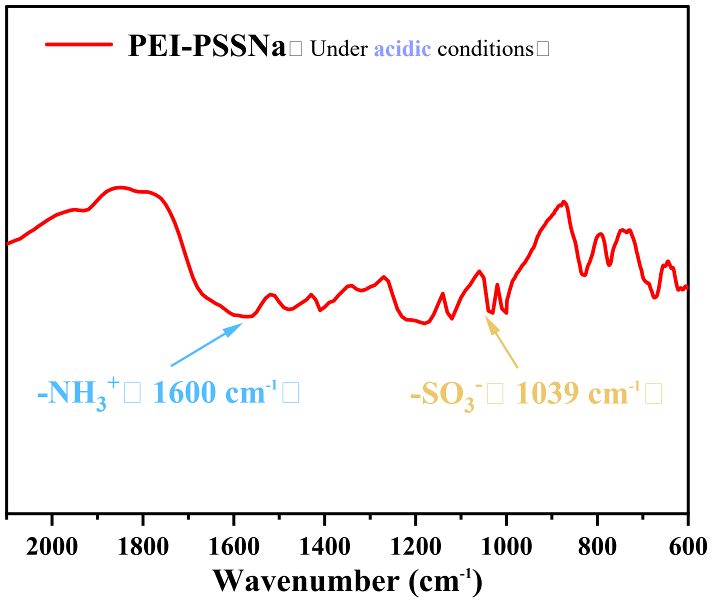

Figure S1. FT-IR spectra of PEI-PSSNa coating under acidic condition.

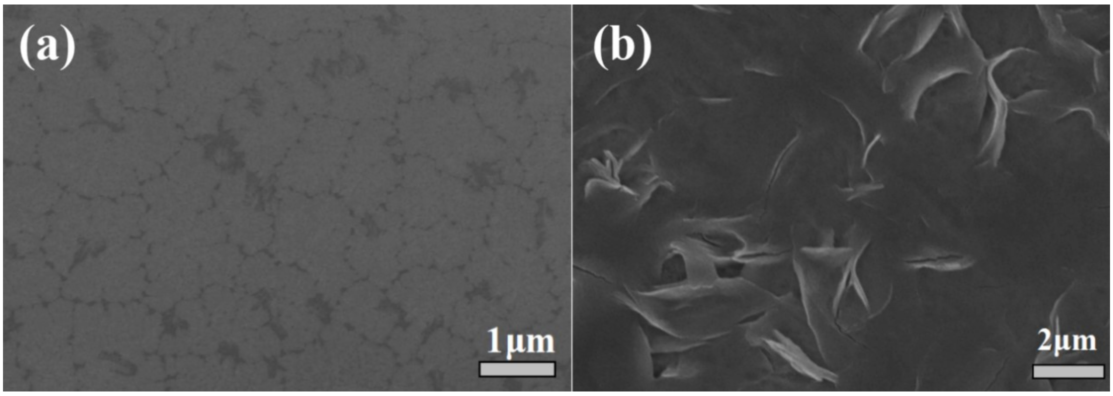

Figure S2. SEM images of PSSNa coatings (a) before and (b) after dropwise addition of 2 M $ZnSO_4$ electrolyte.

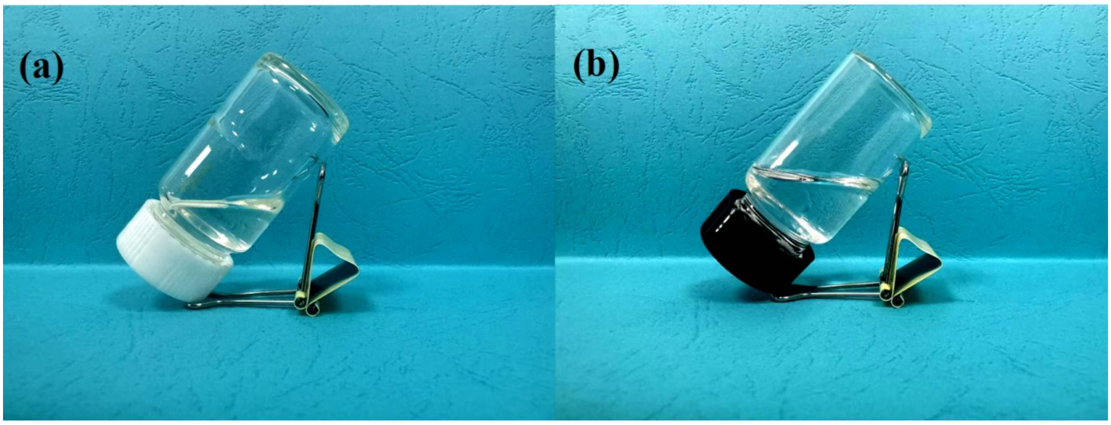

Figure S3. Optical images of (a) PEI-PSSNa solution and (b) PSSNa solution.

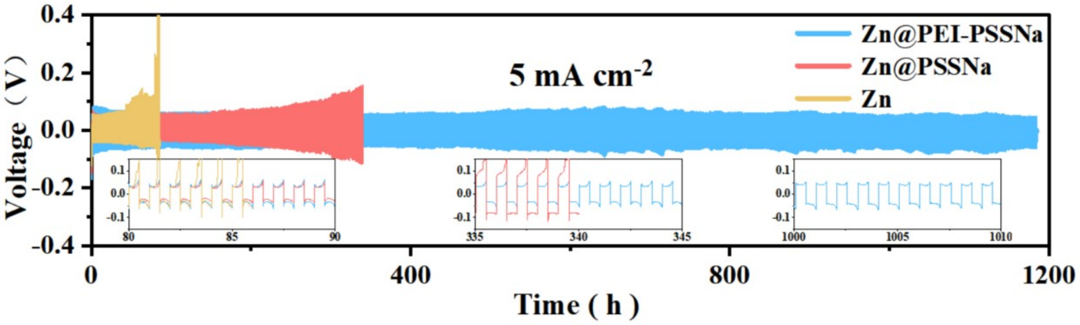

Figure S4. The voltage curves of the symmetric cell during galvanostatic charge - discharge tests under 5 mA cm^{-2} and 2.5 mAh cm^{-2}.

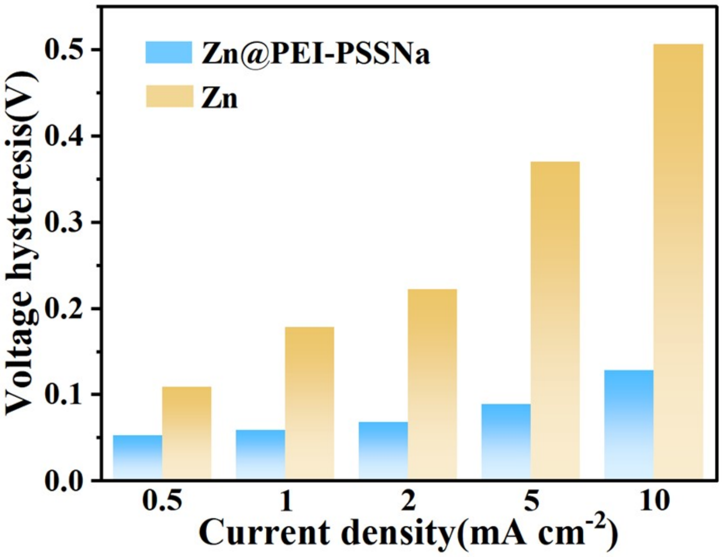

Figure S5. Voltage polarization diagrams in symmetric cell

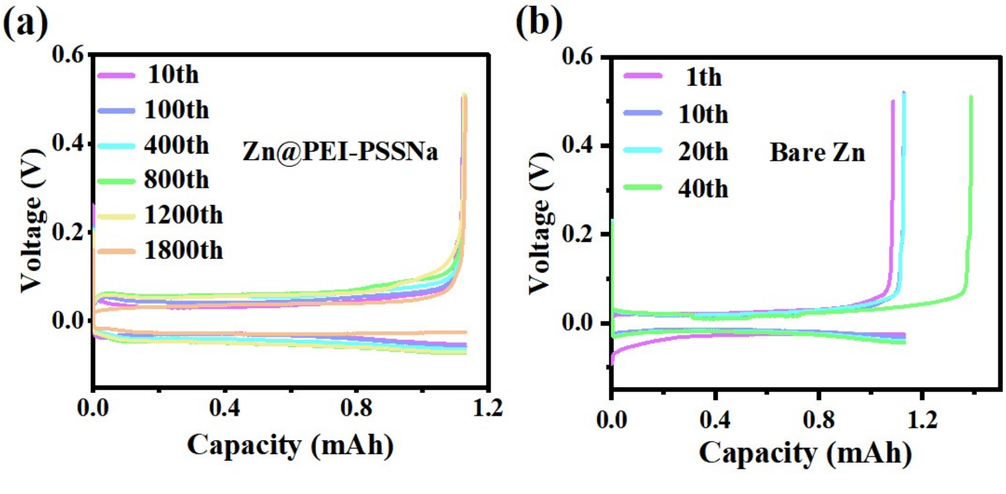

Figure S6. Voltage profiles of (a) Zn||Cu@PEI-PSSNa and (b) Zn||Cu cells at the indicated cycles.

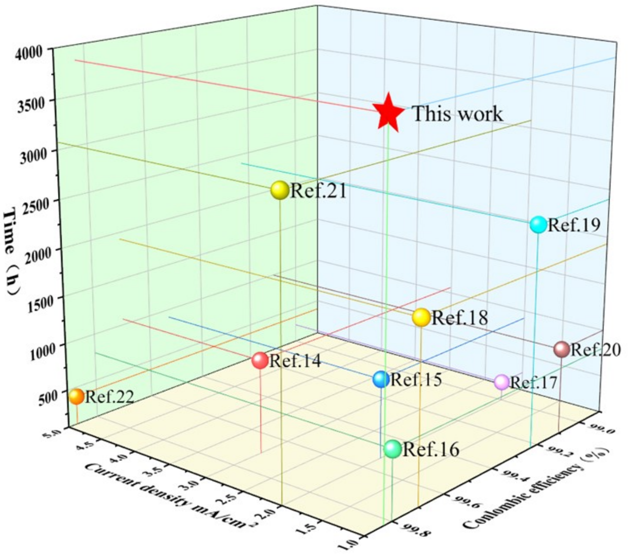

Figure S7. Comparison of the performance of Cu@PEI - PSSNa||Zn cells with previously reported cell performance under anode modification strategies.

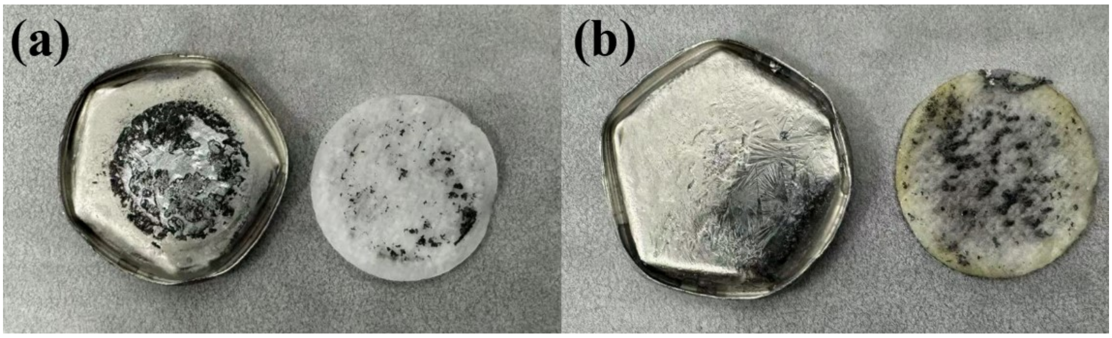

Figure S8. Optical images inside (a) bare Zn symmetric cells and (b) Zn@PEI-PSSNa symmetric cells at high discharge depths.

The data and calculation process related to the DOD are acquired from the followed equations:

$$DOD_{(\%)} = \frac{C_{actual}}{C_{theoretical}} \times 100\% = \frac{I \times t \times S}{m \times C_{theoretical}} \times 100\%$$

In the relevant calculations, the theoretical specific capacity of the zinc anode (approx. 820 mAh g^{-1}) is expressed as $C_{\text{theoretical}}$ (mAh g^{-1}). The specific capacity of the actual deposited/stripped zinc is C_{actual} (mAh g^{-1}). During the plating/stripping process, the current density is expressed as I (mAh cm^{-2}) and the duration of zinc deposition/stripping is expressed as t (h). In addition, the actual area of the electrode is S (cm^2), here 1.13 cm^2, and the mass is m (g), here 8.5 mg.

$$DOD_{(\%)} = \frac{C_{\text{actual}}}{C_{\text{theoretical}}} \times 100\% = \frac{6\,\text{h} \times 1.13\text{mA}}{0.0085\text{g} \times 820\text{mAh/g}} \times 100\% = 97.3\%$$

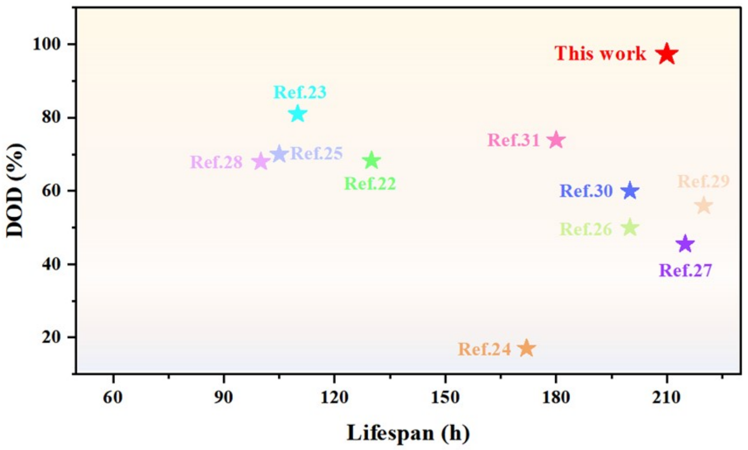

Figure S9. Comparison chart of discharge depth and time with the work of previously published studies.

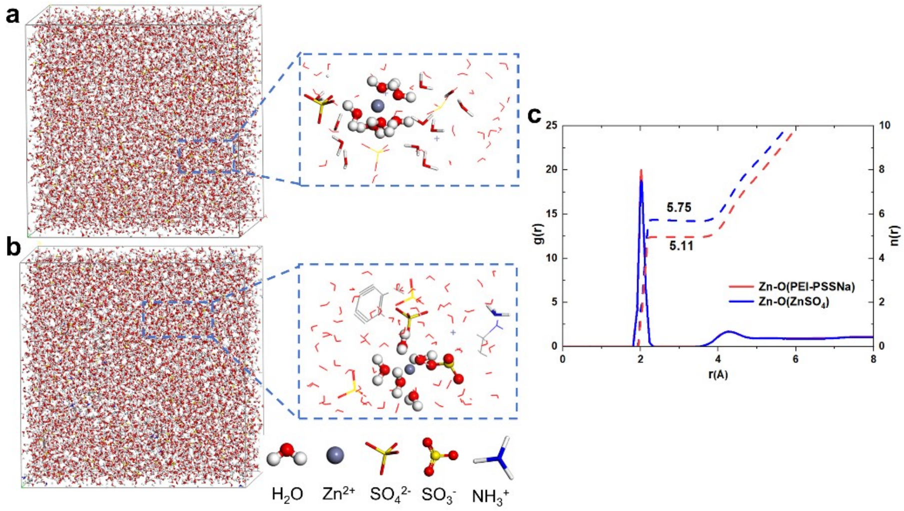

Figure S10. Snapshot of the molecular dynamics (MD) simulations for (a) bare zinc and (b) Zn@PEI-PSSNa electrode/electrolyte interface. (c) the corresponding radial distribution functions (RDFs) obtained from MD simulation.

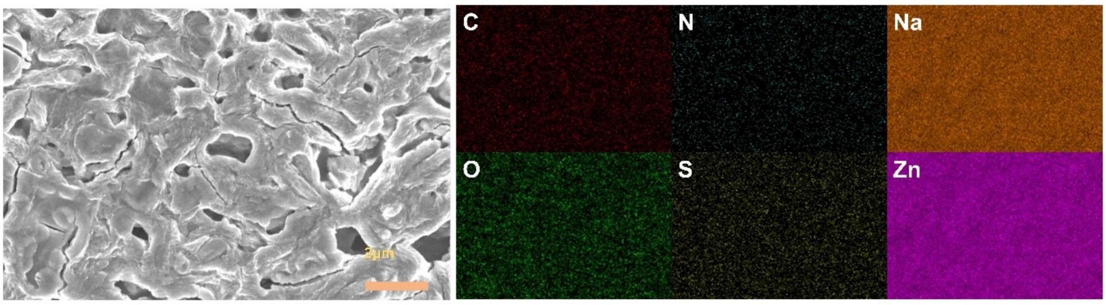

Figure S11. SEM image and element mapping analysis of PEI-PSSNa@Zn anode after 50 cycles at 5 mA cm^{-2} and 2.5 mAh cm^{-2}.

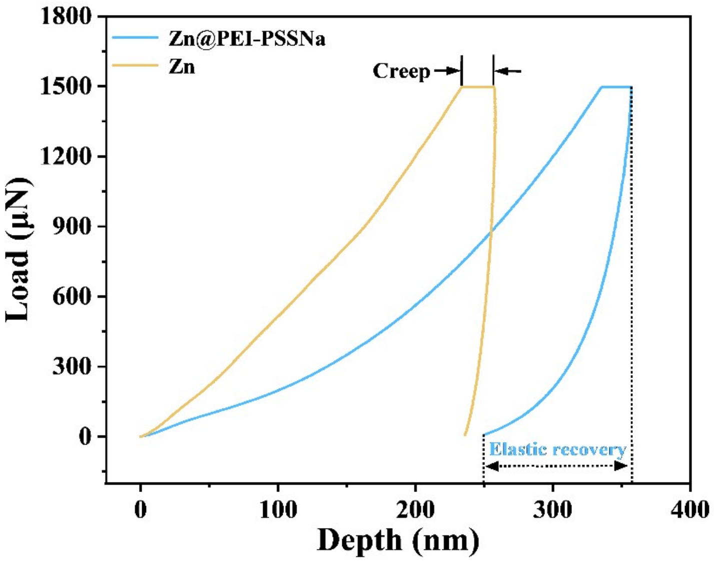

Figure S12. Nanoindentation curves of bare Zn and PEI-PSSNa coating.

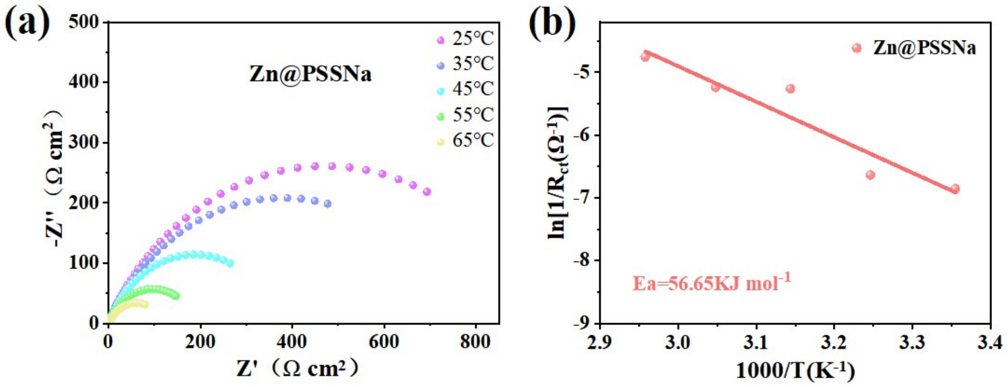

Figure S13. (a) Nyquist plots of Zn@PEI-PSSNa at different temperatures. (b) Corresponding Arrhenius curves.

The activation energy (E_a) is calculated by the Arrhenius equation:

$$\frac{1}{R_{\mathrm{ct}}} = A\exp(-\frac{E_a}{RT})$$

R_{ct} is the charge transfer resistance, R is the molar gas constant, A is the pre-exponential factor, and T is the absolute temperature.

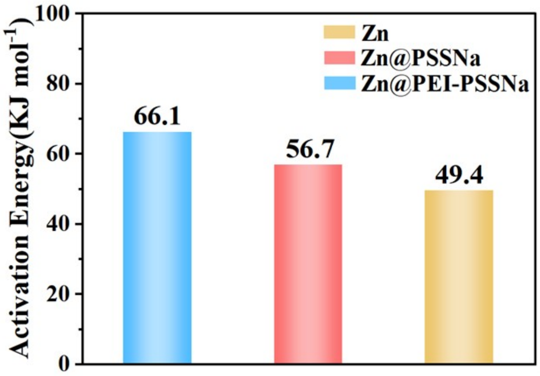

Figure S14. Activation energy of the three groups of samples.

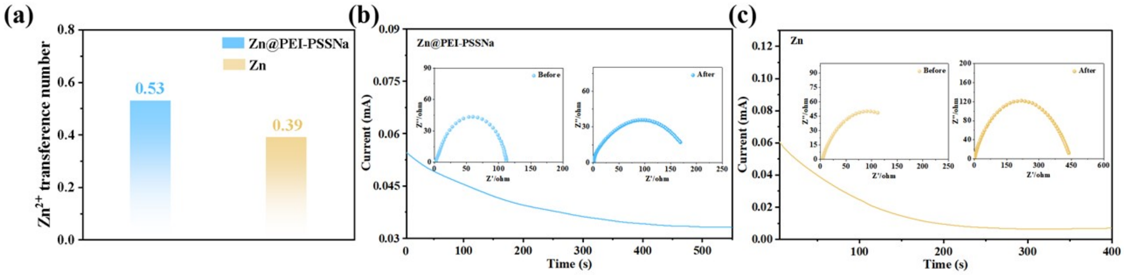

Figure S15. (a) The calculation result of the Zn^{2+} transference number. The (b) and (c) are the specific tests for Zn@PEI-PSSNa and Zn, respectively.

The transference number of Zn^{2+} is calculated by the following formula:

$$t_{Zn^{2+}} = \frac{I_S(\Delta V - I_0 R_0)}{I_0(\Delta V - I_S R_S)}$$

Where ΔV is the constant polarization voltage applied (10 mV), I_0 and R_0 represent the initial current and resistance, while I_s and R_s denote the steady-state current and resistance, respectively.

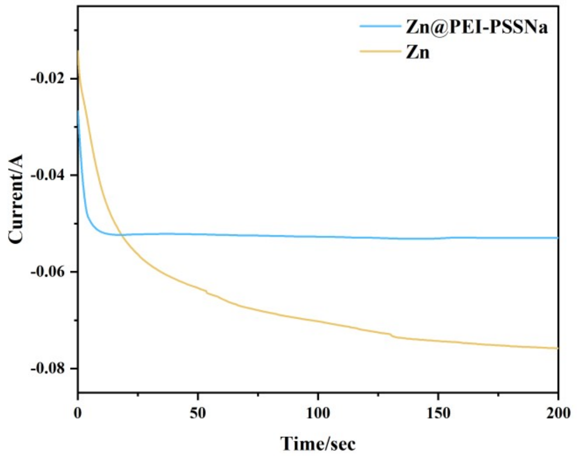

Figure S16. Chronoamperometry (CA) curves of bare Zn and Zn@PEI-PSSNa symmetric cells at a constant potential of -150 mV.

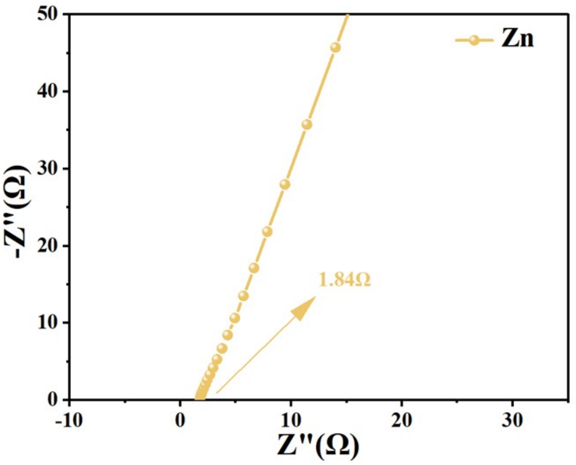

Figure S17. Nyquist diagram for bare Zn.

The ionic conductivity (σ) of the coating is calculated according to the formula

$$\sigma = \frac{L}{R_b S}$$

L is the coating thickness, S is the contact area, and R_b is the coating resistance,

$R_b = (R_{b(coated)} - R_{b(bare)})/2$.

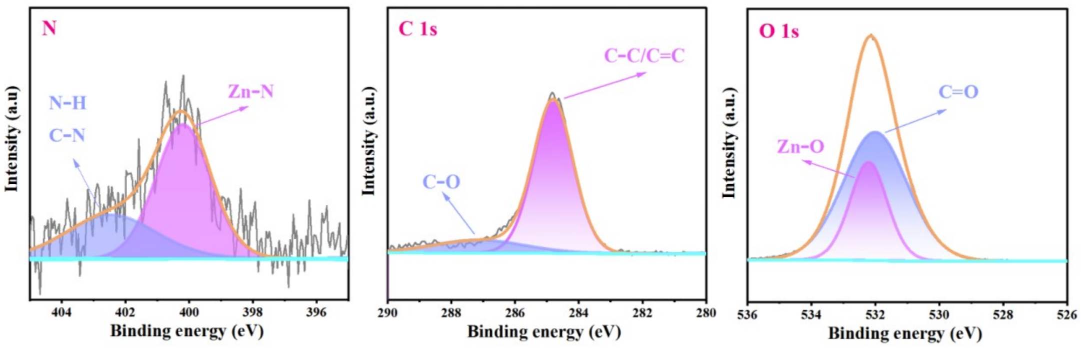

Figure S18. XPS energy spectrum analysis of Zn@PEI-PSSNa electrode after 50 cycles.

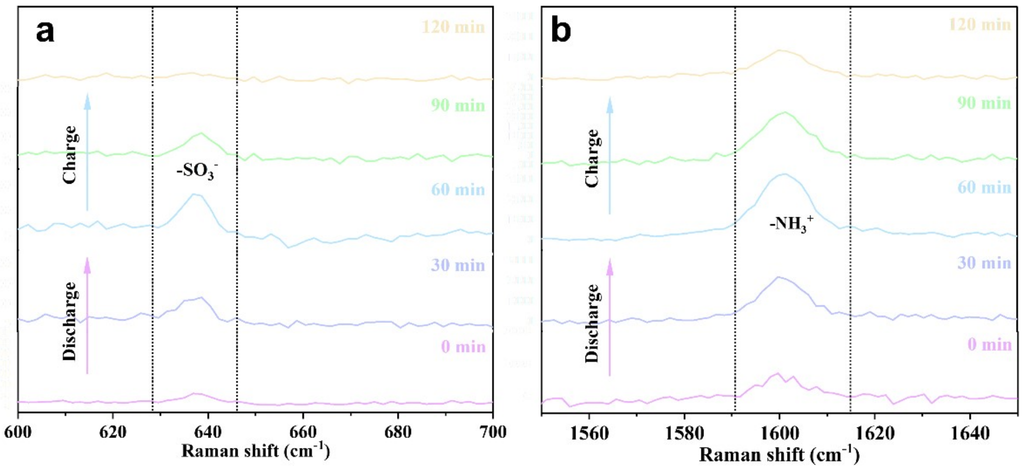

Figure S19. Ex-situ Raman spectra of Zn@PEI-PSSNa electrode at plating/stripping process.

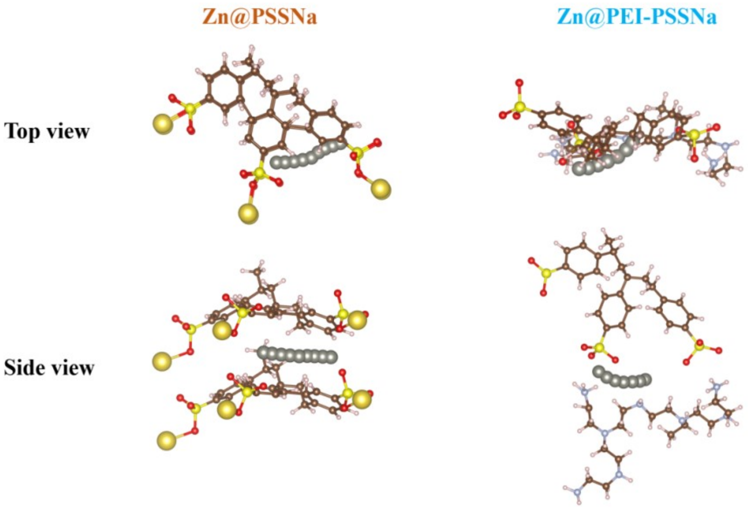

Figure S20. The chemical structure of the sample as observed at different view.

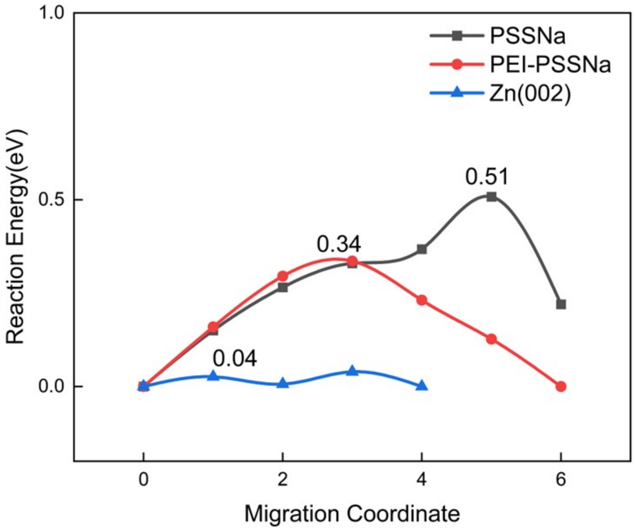

Figure S21. The corresponding diffusion barriers for different samples.

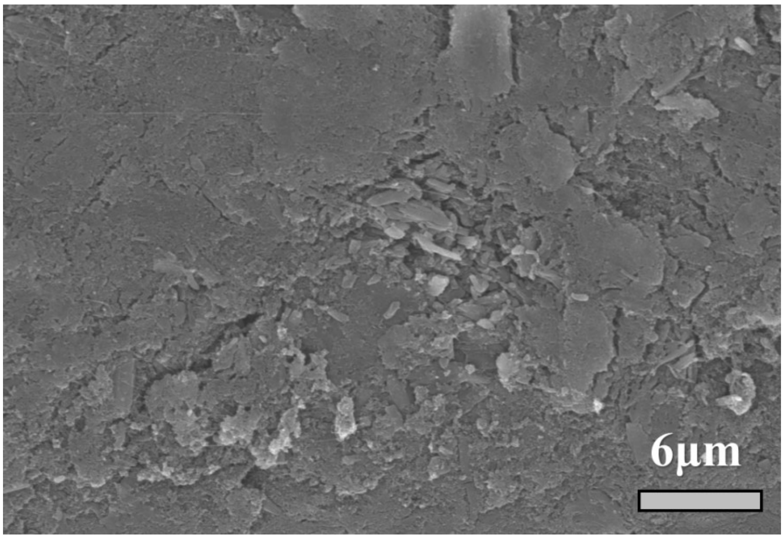

Figure S22. SEM image of the cathode material.

Table S1. Comparison of the performance of symmetric cells with different strategies at high current densities.

Cycle number	**Lifespan (h)**	**Current density ($\mathrm{mA\ cm^{-2}}$)**	**Capacity ($\mathrm{mAh\ cm^{-2}}$)**	**Ref.**
9200	920	40	2	This work
1900	380	10	1	[1]
1212	485	5	1	[2]
5000	1000	10	1	[3]
2250	900	5	1	[4]
840	420	8	2	[5]
7000	700	10	0.5	[6]
2100	420	10	1	[7]
5000	250	40	1	[8]
1600	320	10	1	[9]
500	500	3	1.5	[10]
2200	220	20	1	[11]
2500	1000	10	2	[12]
5800	580	20	1	[13]

Table S2. Comparison of Zn@Cu cell performance under different strategies.

Coating	**Lifespan (h)**	**Current density ($mA\ cm^{-2}$)**	**CE (%)**	**Ref.**
PEI-PSSNa@Zn	3850	1	99.83	This work
TCCF@Zn	1067	3	99.7	[14]
N-TiO@Zn	921	2	99.53	[15]
ZnPO@Zn	800	1	99.8	[16]
ZVO@Zn	300	2	99	[17]
HNT-GF	1930	1	99.7	[18]
PBSC@Zn	2400	1	99.23	[19]
Ti_4O_7@Zn	1000	1	99.1	[7]
LT-Zn@ZnO	3080	2	99.9	[20]
OPA@Zn	400	5	99.87	[21]

Table S3. Comparison with previous strategies in terms of the depth of discharge (DOD) and lifespan.

Journal	**DOD (%)**	**Lifespan (h)**	**Ref.**
★	**97.3**	**210**	**This work**
Adv. Energy Mater.	68.3	130	[22]
Adv. Funct. Mater.	81	110	[23]
Adv. Mater.	17.1	172	[24]
Angew. Chem. Int. Ed.	70	105	[25]
Angew. Chem. Int. Ed.	50	200	[26]
Adv. Mater.	45.5	215	[27]
J. Am. Chem. Soc.	68	100	[28]
Adv. Mater.	56	220	[29]
Adv. Energy Mater.	60	200	[30]
Adv. Funct. Mater.	73.9	180	[31]

Supporting References.

1 P. Lei, L. Liu, X. Wang, Y. Su, K. Yan, B. Wang and J. Cheng, *J. Colloid. Interf. Sci.*, 2025, **679**, 846–854.

2 Q. Ren, X. Tang, X. Zhao, Y. Wang, C. Li, S. Wang and Y. Yuan, *Nano Energy*, 2023, **109**, 108306.

3 Y. Li, Q. Zhu, M. Xu, B. Zang, Y. Wang and B. Xu, *Adv. Funct. Mater.*, 2023, **33**, 2213416.

4 Q. Zong, B. Lv, C. Liu, Y. Yu, Q. Kang, D. Li, Z. Zhu, D. Tao, J. Zhang, J. Wang, Q. Zhang and G. Cao, *ACS Energy Lett.*, 2023, **8**, 2886–2896.

5 B. Sui, L. Sha, Q. Bao, P. Wang, Z. Gong, M. Zhou, F. Shi and K. Zhu, *J. Colloid. Interf. Sci.*,2024, **669**, 886–895.

6 Y. Shen, Y. Liu, K. Sun, T. Gu, G. Wang, Y. Yang, J. Pang, Y. Zheng, X. Yang and L. Chen, *J. Mater. Sci. & Tech.*, 2024, **169**, 137–147.

7 Y. Song, Y. Liu, S. Luo, Y. Yang, F. Chen, M. Wang, L. Guo, S. Chen and Z. Wei, *Adv. Funct. Mater.*, 2024, **34**, 2316070.

8 W. Zhang, W. Qi, K. Yang, Y. Hu, F. Jiang, W. Liu, L. Du, Z. Yan and J. Sun, *Energy Storage Mater.*, 2024, **71**, 103616.

9 M. Abouali, S. Adhami, S. A. Haris and R. Yuksel, *Angew. Chem. Int. Ed.*, 2024, **63**, e202405048.

10 B. Li, S. Liu, Y. Geng, C. Mao, L. Dai, L. Wang, S. C. Jun, B. Lu, Z. He and J. Zhou, *Adv. Funct. Mater.*, 2024, **34**, 2214033.

11 J. Zhou, Y. Mei, F. Wu, Y. Hao, W. Ma, L. Li, M. Xie and R. Chen, *Angew. Chem. Int. Ed.*, 2023, **62**, e202304454.

12 W. Xie, K. Zhu, W. Jiang, H. Yang, M. Ma, L. Zhao and W. Yang, *ACS Nano*, 2024, **18**, 21184–21197.

13 Y. Ai, C. Yang, Z. Yin, T. Wang, T. Gai, J. Feng, K. Li, W. Zhang, Y. Li, F. Wang, D. Chao, Y. Wang, D. Zhao and W. Li, *J. Am. Chem. Soc.*, 2024, **146**, 15496–15505.

14 P. Wu, L. Xu, X. Xiao, X. Ye, Y. Meng and S. Liu, *Adv. Mater.*, 2024, **36**, 2306601.

15 Y. Huyan, Z. Luo, Z. Hou, M. Jiang, C. Wei and J.-G. Wang, *Energy Storage Mater.*, 2024, **72**, 103702.

16 S. Xia, Q. Luo, J. Liu, X. Yang, J. Lei, J. Shao and X. Tang, *Small*, 2024, **20**, 2310497.

17 G. Yoo, Y.-R. Jo and G.-H. An, *ACS Energy Lett.*, 2024, **9**, 5955–5965.

18 S. Liu, Q. Han, C. He, Z. Xu, P. Huang, L. Cai, H. Chen, H. Zheng, Y. Zhou, M. Wang, H. Tian, W.-Q. Han and H. Ying, *ACS Nano*, 2024, **18**, 25880–25892.

19 Y. Guo, C. Luo, M. Yang, H. Wang, W. Ma, K. Hu, L. Li, F. Wu and R. Chen, *Angew. Chem. Int. Ed.*, 2024, **63**, e202406597.

20 Z. Cheng, J. Fu, P. Kang, H. Yao, F. Mo and H. Hu, *Adv. Energy Mater.*, 2025, 2405767.

21 T. Li, S. Yan, H. Dong, Y. Zheng, K. Ming, Y. Chen, H. Li, G. Li, Z. He, W. Li, Q. Wang, X. Song, J. Liu, E. H. Ang and Y. Wang, *J. Energy Chem.*, 2024, **97**, 1–11.

22 Y. Chen, S. Zhou, J. Li, J. Kang, S. Lin, C. Han, H. Duan, S. Liang and A. Pan, *Adv. Energy Mater.*, 2024, **14**, 2400398.

23 P. Cao, X. Zhou, A. Wei, Q. Meng, H. Ye, W. Liu, J. Tang and J. Yang, *Adv. Funct. Mater.*, 2021, **31**, 2100398.

24 X. Yang, C. Li, Z. Sun, S. Yang, Z. Shi, R. Huang, B. Liu, S. Li, Y. Wu, M. Wang, Y. Su, S. Dou and J. Sun, *Adv. Mater.*, 2021, **33**, 2105951.

25 J. Ji, H. Du, Z. Zhu, X. Qi, F. Zhou, R. Li, R. Jiang, L. Qie and Y. Huang, *Angew. Chem. Int. Ed.*, 2025, **64**, e202414562.

26 P. Sun, Z. Cao, Y. Zeng, W. Xie, N. Li, D. Luan, S. Yang, L.Yu and X. Lou, *Angew. Chem. Int. Ed.,* 2022, **61**, 2115649.

27 J. Zhang, W. Huang, L. Li, C. Chang, K. Yang, L. Gao and X. Pu, *Adv. Mater.,*2023, **35**, 2300073.

28 F. Ming, Y. Zhu, G. Huang, A.-H. Emwas, H. Liang, Y. Cui and H. N. Alshareef, *J. Am. Chem. Soc.*, 2022, **144**, 7160–7170.

29 X. Zhang, J. Li, K. Qi, Y. Yang, D. Liu, T. Wang, S. Liang, B. Lu, Y. Zhu and J. Zhou, *Adv. Mater.*, 2022, **34**, 2205175.

30 B. Liu, X. Ma, Q. Wang, S. Zhang, J. Yuwono, H. Jin, J. Qiu, H. Ma, C. Wang and C. Lai, *Adv. Energy Mater.*, 2024, 2404660.

31 K. Wang, H. Zhan, X. Liu and X. Sun, *Adv. Funct. Mater.*, 2024, 2418993.